Terahertz Conductivity and Possible Bloch Gain in Semiconductor Superlattices

Y. Shimada* and K. Hirakawa†
Institute of Industrial Science, University of Tokyo, 4-6-1 Komaba, Meguro-ku, Tokyo 153-8505, Japan

M. Odnoblioudov and K. A. Chao
Division of Solid State Theory, Department of Physics, Lund University, S-233 62, Sweden
(Received 19 August 2002; published 30 January 2003)

We have investigated terahertz emission due to dynamical electron transport in wide-miniband $GaAs/Al_{0.3}Ga_{0.7}As$ superlattices. By noting that the time-domain THz emission spectroscopy inherently measures the step-response of the electron system to the bias electric field, the obtained THz spectra were compared with the high-frequency conductivities predicted for miniband transport. Excellent agreement between theory and experiment strongly supports that the THz gain due to Bloch oscillating electrons persists at least up to 1.7 THz. It was also found that Zener tunneling into the second miniband sets the high-frequency limit to the THz gain for the samples studied here.

DOI: 10.1103/PhysRevLett.90.046806 PACS numbers: 73.63.Hs, 73.21.Cd, 73.50.Mx, 78.47.+p

Since the first proposal by Esaki and Tsu [1] that artificial band structures in semiconductor superlattices (SLs) should support Bloch oscillations (BOs), considerable effort from both experiments [2–11] and theories [12,13] has been made to search for BOs and obtain terahertz emission. Ultrafast time-domain experiments unambiguously demonstrate that electrons in SL minibands perform at least a few cycle BOs [7–11]. However, the idea of the Bloch oscillator was challenged by asking whether BO is useful in generating/amplifying electromagnetic (EM) waves [14]. When an electric field is applied to an ideal SL, the miniband is split into equally spaced Wannier-Stark (WS) ladder states with an energy separation of $\hbar\omega_B$ (ω_B the Bloch frequency and $\hbar$ the reduced Planck constant). Since the emission and absorption of EM waves take place between the adjacent two WS levels, they occur at the same frequency and, hence, cancel each other. Consequently, an ideal SL has no net gain or loss for EM waves. However, when scattering exists in the system, new transition channels, i.e., scattering-assisted transitions, become available. Since the scattering-assisted emission (absorption) occurs at frequencies slightly lower (higher) than ω_B, gain (loss) for EM waves is expected below (above) ω_B.

The direct experimental proof of such THz gain is to show that the real part of the carrier conductivity, $\mathrm{Re}[\sigma(\omega)]$, becomes negative in the THz range. The conventional method for determining $\mathrm{Re}[\sigma(\omega)]$ in the THz range is the measurement of free carrier absorption in doped SLs under bias electric fields by using, for example, Fourier transform spectrometers [3]. Here, fundamental problems arise: (i) For such measurements, a large sample size, typically a few mm^2, is necessary. Then, an extremely large current flows through the sample under biased conditions. (ii) The profile of internal electric field in doped SLs becomes very nonuniform due to the formation of high-field domains. These two inevitable problems have made the conventional measurements practically impossible so far.

In this Letter, we present strong experimental support for the THz gain due to Bloch oscillating electrons in wide-miniband $GaAs/Al_{0.3}Ga_{0.7}As$ SLs. For determining the high-frequency electron conductivity in SL minibands, we took a totally different approach; we used undoped SL samples in order to avoid large current density and high-field domain formation and took all the necessary information within a few ps, by noting that the time-domain THz spectroscopy inherently measures the step-response of the electron system to the applied bias electric field and that the Fourier spectra of the THz emission is closely related with $\sigma(\omega)$. Quasi-autocorrelation measurements were performed on the emitted THz electromagnetic wave, and the obtained spectra were compared with $|\sigma(\omega)|^2$ predicted theoretically [12]. Although we do not directly show a negative $\mathrm{Re}[\sigma(\omega)]$, excellent agreement between theory and experiment on $|\sigma(\omega)|^2$ spectra strongly suggests that the THz gain due to Bloch oscillating electrons persists at least up to 1.7 THz.

The samples used in this work were $GaAs/Al_{0.3}Ga_{0.7}As$ SL *m-i-n* (metal-intrinsic-n^+-type) diode structures. Two different wide-miniband SL samples were prepared by growing undoped $GaAs/Al_{0.3}Ga_{0.7}As$ SL layers (sample No. 1: 8.2 nm/0.8 nm and sample No. 2: 6.4 nm/0.56 nm) on n^+-GaAs substrates by molecular beam epitaxy. The first miniband widths, Δ, of the two samples were designed to be 50 and 100 meV, respectively. For both samples, the second miniband was separated by a 40-meV-wide minigap. The thickness of the undoped SL layers was 500 nm. The top contacts were formed by depositing semitransparent 4-nm-thick NiCr Schottky films and the bottom Ohmic contacts were formed by annealing AuGeNi alloy. By applying a bias voltage, V_b, between the top and the bottom electrodes, we can

tune an internal electric field, F, in the undoped SL region. When a femtosecond laser pulse excites the sample, electron-hole pairs are optically injected into the miniband. Because of an applied electric field, F, the carriers start drifting and THz radiation that is proportional to the carrier acceleration is emitted into free space. Since the hole miniband is much narrower, holes are almost localized under biased conditions. Consequently, electron motion dominates the emitted THz signal.

To verify the formation of the miniband and the WS ladder in our samples, we first took weak-excitation interband photocurrent spectra, I_{ph}. Figure 1(a) shows the contour plot of the derivative of I_{ph}, i.e., $dI_{ph}/dh\nu$, measured on sample No. 1 ($\Delta = 50$ meV), where $h\nu$ is the incident photon energy. For $+0.8\ \mathrm{V} > V_b > +0.5\ \mathrm{V}$, only an excitonic absorption at the bottom of the miniband is observed. However, when V_b is reduced below

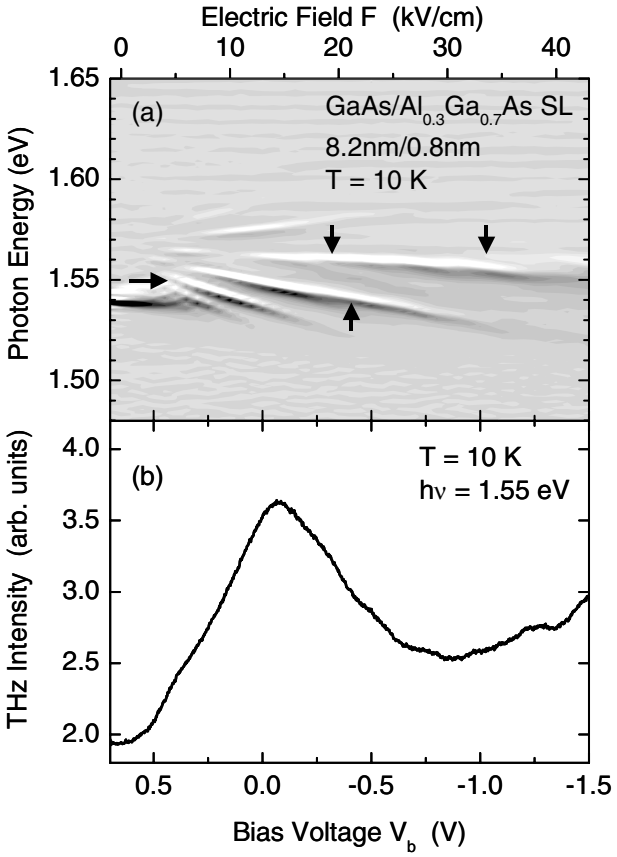

FIG. 1. (a) The contour plot of the derivative spectra of the interband photocurrent, $dI_{ph}/d\hbar\nu$, measured on sample No. 1 as a function of the applied bias voltage. The horizontal arrow denotes the photon energy of the femtosecond laser pulses used for the time-domain THz measurements. The vertical arrows indicate the anticrossing points due to Zener tunneling into the second miniband. (b) The integrated intensity of the THz emission is plotted as a function of the bias voltage.

$+0.5$ V, the spectrum starts showing rich structures which originate from the formation of the WS ladder.

For time-domain THz emission spectroscopy, we used a quasiautocorrelation geometry, i.e., the power of the THz radiation generated by a pair of time-correlated femtosecond laser pulses was measured as a function of the time interval, t, between the two laser pulses imposed by a Michelson interferometer. Experiments were performed by using 100 fs laser pulses delivered from a mode-locked Al_2O_3:Ti laser. The laser pulses were loosely focused onto the sample surface. The pump power, P, used in the experiment was 10 mW. The pump photon energy was set to be 1.55 eV, which is close to the bottom of the miniband, as indicated by the horizontal arrow in Fig. 1(a) [11]. The generated THz emission was detected by a wideband Si bolometer. The samples were cooled at 10 K.

Figure 1(b) shows the integrated intensity of the emitted THz radiation as a function of V_b measured for sample No. 1. The THz intensity starts rising at about $V_b = +0.65$ V, indicating that this voltage is the flatband voltage, V_{b0}, in this particular sample. With decreasing V_b (i.e., increasing reverse bias), the THz intensity increases first. However, when the reverse bias exceeds -0.1 V, the THz intensity starts to roll off due to the field-induced Stark localization [11].

Figure 2(a) plots the autocorrelation traces of the emitted THz radiation measured at various F for sample No. 1. F was estimated from V_{b0} and the total thickness of the undoped SL layer. At very low fields, a hump is seen at about $t = 0$. However, as we increase F, a few cycle oscillations start to show up. From the F dependence of the oscillation frequency, the observed oscillations were identified as BOs. The Fourier spectra of the time-domain traces are plotted in Fig. 2(b). As seen in the figure, the peak position of the BO shifts to higher frequency as F is increased. However, for $F > 17$ kV/cm, the spectral shape drastically changes and becomes very broad. The behavior in the large reverse bias region will be discussed later.

At this stage, we discuss what the THz emission spectra represent. In the THz emission experiment, we first set a dc electric field F in the SL and then shoot a fs-laser pulse to the sample at $t = 0$ to create a step-function-like carrier density, $n\Theta(t)$, in the sample. Subsequently, THz radiation is emitted from the accelerated photoexcited electrons. Now, by using our imagination, we view the experiment in a different way. Let us perform the following thought experiment; we first set electrons in the conduction miniband under a flatband condition and, at $t = 0$, suddenly apply a step-function-like bias electric field, $F\Theta(t)$. We notice that electrons in the thought experiment emit the same THz radiation as in the actual experiment. This fact implies that the time-domain THz experiment inherently measures the step-response of the electron system to the applied electric field.

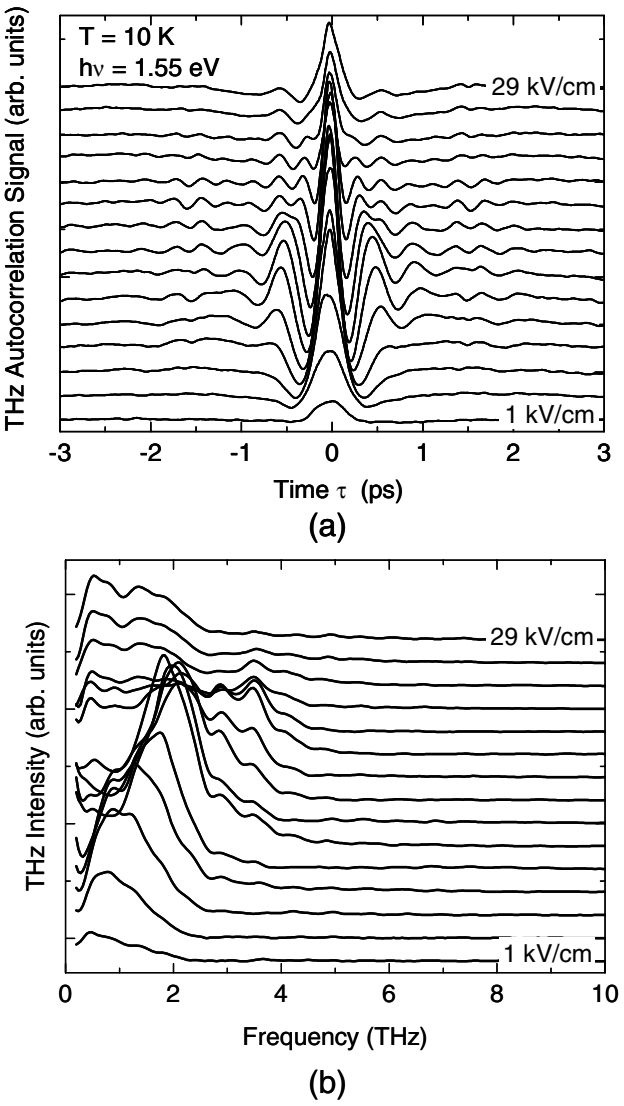

FIG. 2. (a) The autocorrelation traces of the THz emission and (b) their Fourier spectra measured on sample No. 1 for various bias electric fields from 1 kV/cm to 29 kV/cm with a 2 kV/cm step. The traces are shifted for clarity.

By noting this important conclusion, we formulate the THz emission process as follows: the creation of step-function-like carrier density by fs-laser pulses in the actual process is replaced with the application of step-function-like electric field in the thought experiment as

$$F(t) = F\Theta(t), \qquad \tilde{F}(s) = \frac{F}{s}. \tag{1}$$

Here, the variables with ˜ denote their Laplace transformation. The transient current by the photoexcited electrons in the miniband is given by

$$\tilde{J}(s) = \tilde{\sigma}(s)\tilde{F}(s). \tag{2}$$

Then the emitted THz electric field, E_{THz}, can be obtained as

$$E_{\mathrm{THz}} \propto \frac{\partial J(t)}{\partial t} = \frac{1}{2\pi i}\int_{c-i\infty}^{c+i\infty} s e^{ts}\tilde{\sigma}(s)\frac{F}{s}ds = \sigma(t)F, \tag{3}$$

where $\sigma(t)$ is the electron conductivity in the time domain. Equation (3) tells us that, since the spectra shown in Fig. 2(b) are the Fourier spectra of the THz autocorrelation traces, they are proportional to $|\sigma(\omega)|^2F^2$.

In the following, we compare the observed THz spectra with the conductivity theoretically predicted for the Bloch oscillating electrons by Ktitrov *et al.* [12]:

$$\sigma(\omega) = \sigma_0\frac{1 - \omega_B^2\tau_m\tau_e - i\omega\tau_e}{(\omega_B^2 - \omega^2)\tau_m\tau_e + 1 - i\omega(\tau_m + \tau_e)}$$
$$\text{with} \quad \sigma_0 = \frac{\sigma_{00}}{1 + \omega_B^2\tau_m\tau_e}, \tag{4}$$

where τ_m and τ_e are the momentum and energy relaxation times of electrons, respectively, and σ_{00} a constant. The top panels of Fig. 3 show the calculated real and imaginary parts of the miniband conductivity, and the bottom panels show the measured THz spectra and calculated $|\sigma(\omega)|^2$ for two representative bias conditions. τ_m and τ_e in the calculation were determined to be 0.15 and 1.5 ps, respectively, from numerical fitting. ω_{B} at $F =$ 1.0 kV/cm was simply set to be $edF/\hbar$. However, we found that the peak position of the THz spectrum at 11.1 kV/cm is slightly lower than the value simply expected from $edF/\hbar$ (2.41 THz), which is due to anticrossing with the WS ladder states of the second miniband, as will be discussed later. We set ω_{B} at $F = 11.1$ kV/cm to be 1.96 THz, which gives the best fit to the experimental data.

At very low field [$F = 1.0$ kV/cm, $\omega_{\mathrm{B}}(\tau_m\tau_e)^{0.5} =$ 0.66], the conductivity spectra and the THz emission

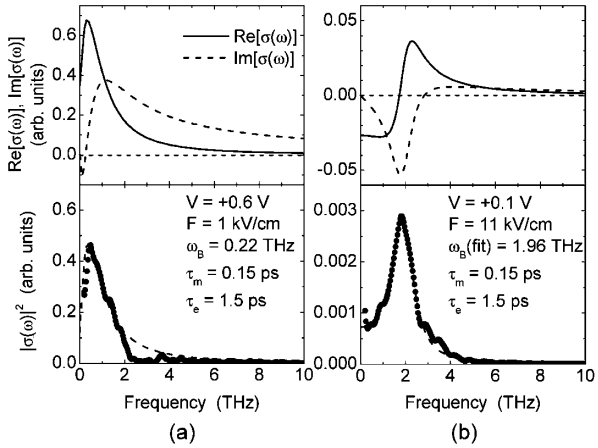

FIG. 3. The top panels show the calculated real (solid line) and imaginary (dashed line) parts of $\sigma(\omega)$ for the superlattice miniband. The bottom panels show the calculated $|\sigma(\omega)|^2$ spectra (dashed line) and the THz emission spectra (dots) measured for sample No. 1 by the time-domain THz spectroscopy; (a) $F = 1.0$ kV/cm and (b) $F = 11$ kV/cm.

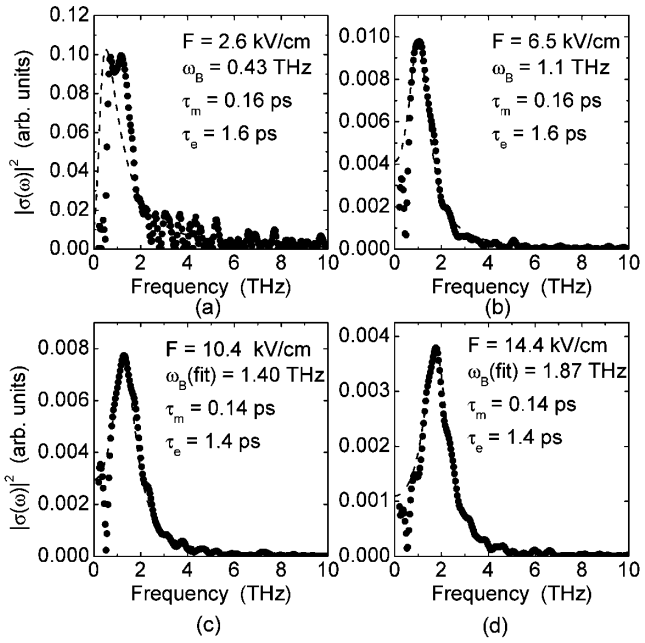

FIG. 4. The calculated $|\sigma(\omega)|^2$ spectra (dashed line) and the THz emission spectra (dots) measured for sample No. 2 are shown for four bias electric fields: (a) 2.6 kV/cm, (b) 6.5 kV/cm, (c) 10.4 kV/cm, and (d) 14.4 kV/cm. The sharp dips at 0.5 THz in the measured data are due to water vapor absorption.

show more or less a Drude-like behavior [see Fig. 3(a)]. However, as F is increased, Eq. (4) predicts that a negative $\mathrm{Re}[\sigma(\omega)]$ below ω_B develops and that a clear dip in $\mathrm{Im}[\sigma(\omega)]$ appears at ω_B. Consequently, the expected $|\sigma(\omega)|^2$ spectrum becomes asymmetric with an enhanced low-frequency spectral component. It should be noted in Fig. 3(b) that the THz emission at $F = 11.1$ kV/cm $[\omega_B(\tau_m\tau_e)^{0.5} = 5.8]$ indeed has a characteristic asymmetric spectral shape and that the agreement between the observed THz emission and the calculated $|\sigma(\omega)|^2$ is excellent, indicating that E_{THz} is indeed proportional to $\sigma(\omega)$ of Bloch oscillating electrons. Furthermore, the calculated $\mathrm{Re}[\sigma(\omega)]$ strongly suggests that the THz gain persists at least up to 1.7 THz. Similar experiments were performed for sample No. 2 ($\Delta = 100$ meV). Figure 4 summarizes the THz spectra and the calculated $|\sigma(\omega)|^2$ for various F. Except for the case at $F =$ 2.6 kV/cm, where the THz emission is quite weak and the signal/noise ratio is low, the excellent agreement between experiment and theory further confirms the above conclusion.

When F is further increased, however, the THz spectra suddenly change their spectral shapes, as seen in Fig. 2(b). We attribute this behavior to the Zener tunneling into the higher miniband. Let us take a look at Fig. 1(b) again. It is noted that the THz emission becomes brighter with increasing field for $F > 29$ kV/cm. This fact contradicts what is expected from simple field-induced Stark localization in a single miniband and indicates that electrons in the first miniband find a new conduction channel by Zener tunneling. Further support can be seen in the interband photocurrent spectra shown in Fig. 1(a), where anticrossing with the WS states of the second miniband can be observed in the high bias region, as indicated by vertical arrows [15]. From these data, it is concluded that the Zener tunneling into the higher miniband set the high-frequency limit to the Bloch gain.

In summary, we have investigated THz emission due to dynamical electron transport in wide-miniband GaAs/$Al_{0.3}Ga_{0.7}As$ SLs by time-domain THz emission spectroscopy. The obtained THz spectra were compared with theoretically predicted high-frequency conductivities in SLs. Excellent agreement between theory and experiment strongly supports that the THz gain due to Bloch oscillating electrons in wide-miniband superlattices persists at least up to 1.7 THz.

The authors thank G. Bastard, S. Madhavi, H. Sakaki, and Y. Arakawa for fruitful discussions. This work was supported by CREST of JST, the Grant-in-Aid from JSPS (No. 12450140), and the Grant-in-Aid for COE research from MEXT (No. 12CE2004).

*Present address: AIST, 1-1-1 Umezono, Tsukuba, Ibaraki 305-8563, Japan.
†Electronic address: hirakawa@iis.u-tokyo.ac.jp

[1] L. Esaki and R. Tsu, IBM J. Res. Dev. **14**, 61 (1970).
[2] E. E. Mendez, F. Agullo-Rueda, and M. Hong, Phys. Rev. Lett. **60**, 2426 (1988).
[3] S. J. Allen *et al.*, Semicond. Sci. Technol. **7**, B1 (1992).
[4] M. Helm, Semicond. Sci. Technol. **10**, 557 (1995).
[5] K. Unterrainer *et al.*, Phys. Rev. Lett. **76**, 2973 (1996).
[6] E. Schomburg *et al.*, Phys. Rev. B **58**, 4035 (1998).
[7] J. Feldmann *et al.*, Phys. Rev. B **46**, 7252 (1992).
[8] C. Waschke *et al.*, Phys. Rev. Lett. **70**, 3319 (1993).
[9] T. Dekorsy *et al.*, Phys. Rev. B **50**, 8106 (1994).
[10] F. Löser *et al.*, Phys. Rev. B **61**, R13 373 (2000).
[11] Y. Shimada, K. Hirakawa, and S.-W. Lee, Appl. Phys. Lett.**81**, 1642 (2002).
[12] S. A. Ktitorov, G. S. Simin, and V. Ya. Sindalovskii, Sov. Phys. Solid State **13**, 1872 (1972).
[13] A. A. Ignatov, K. F. Renk, and E. P. Dodin, Phys. Rev. Lett. **70**, 1996 (1993).
[14] G. Bastard and R. Ferreira, C. R. Acad. Sci., Ser. II: Mec., Phys., Chim., Sci. Terre Univers **312**, 971 (1991).
[15] B. Rosam *et al.*, Phys. Rev. Lett. **86**, 1307 (2001).